

**MINISTRY OF EDUCATION  
AND TRAINING**

**VIETNAM ACADEMY OF SCIENCE AND  
TECHNOLOGY**

**GRADUATE UNIVERSITY OF SCIENCE AND TECHNOLOGY**



**Phan Minh Vuong**

**SYNTHESIS AND MODIFICATION OF LAYERD DOUBLE  
HYDROXIDES AND THEIR APPLICATION IN CORROSION  
PROTECTION OF STEEL BASED ON EPOXY COATING**

**SUMMARY OF DISSERTATION ON SCIENCES OF MATTER**

**Major: Theoretical and physical chemistry**

**Code: 9 44 01 19**

**Ho Chi Minh city - 2024**

The dissertation is completed at: Graduate University of Science and Technology, Vietnam Academy Science and Technology

Supervisors:

Supervisor 1: Dr. Phan Thanh Thao, Institute of Chemical Technology

Supervisor 2: Assoc. Prof. Dr. To Thi Xuan Hang, Institute for Tropical Technology

Reviewer 1: Assoc. Prof. Dr. Le Viet Hai, University of Science – Viet Nam national University Ho Chi Minh city

Reviewer 2: Assoc. Prof. Dr. Tran Nguyen Minh An, Industrial University of Ho Chi Minh city – Ministry of Industry & Trade

Reviewer 3: Assoc. Prof. Dr. Tran Quang Hieu, Saigon Technology University – Ministry of Education and Training

The dissertation is examined by Examination Board of Graduate University of Science and Technology, Vietnam Academy of Science and Technology at 14h00, date 22/11/2024.

The dissertation can be found at:

1. Graduate University of Science and Technology Library
2. National Library of Vietnam

## INTRODUCTION

### 1. The urgency of the thesis

Layered double hydroxide (LDH), also known as anion clay, is a layered structure material with anion exchange properties. It is used as a carrier capable of retaining functional anions and releasing them upon exposure to a suitable environment. However, the natural aggregation of LDH crystals during synthesis hinders the comprehensive contact of the corrosive environment with the double layers where the anions are stored. This limits the diffusion of corrosion-inhibiting anions into the environment, thus reducing the anion exchange capacity and the inhibition efficiency. Therefore, the controlled synthesis of LDH is crucial to enhance the inherent properties of the material. Additionally, controlling the stacking of hydroxide layers will facilitate the synthesis of LDH materials with a 2D structure, forming ultra-thin nanosheets with thicknesses ranging from 0.5 nm to 3 nm. In this state, LDH nanosheets exhibit high anisotropy, offering special physical and chemical effects. In the context of corrosion prevention, LDH nanosheets demonstrate superior corrosion inhibitor carrying capacity compared to bulk LDH materials.

In this thesis, the goal is to fabricate LDH nanosheets with controlled morphology and size. The research focuses on controlling the factors influencing the formation and growth of LDH crystals. The even and discrete development of LDH is managed through the treatment of seed microcrystals, a process not yet clarified in current studies. This includes steps such as separating the nuclei from the mother solution and dispersing aggregated nuclei clusters into individual nuclei using high-speed homogenization techniques. Based on these individual nuclei, it is possible to create uniformly shaped LDH nanosheets through a stirred hydrothermal treatment process.

Simultaneously, the research also focuses on synthesizing a nanosheet system carrying the corrosion inhibitor 2-benzothiazolythio-succinic acid (BTSA) through anion exchange methods. With its thin, discrete, and uniform layered

structure, the resulting LDH nanocontainers can arrange uniformly and directionally within polymer membranes, thereby enhancing the resistance to corrosive anion penetration on metal surfaces and improving the effectiveness of organic coatings. From the above analysis, the thesis titled **“Synthesis and modification of layered double hydroxides and their application in corrosion protection of steel based on epoxy coating”** aims to contribute to a new direction in synthesizing ultra-thin 2D LDH layered materials with advanced technology and the potential for pilot-scale production. Consequently, the thesis also provides valuable experimental data and scientific foundations in the field of research, fabrication, and application of 2D LDH materials in Vietnam, aiming to keep up with global trends in advanced material applications, particularly in corrosion protection.

## **2. Objective of the thesis**

The main objective of the thesis is to determine the conditions for successfully synthesizing the ultra-thin nanosheet MgAl layered double hydroxide (LDH) material system with:

- (1) Uniform morphology, LDH crystal phase with low unit cell (2~3 single layers), and particle thickness less than 3.0 nm. The LDH nanosheet particles should have a narrow size distribution, controlled within the range of 50 – 250 nm depending on hydrothermal conditions.
- (2) High organic corrosion inhibitor loading capacity (>30%) and high corrosion inhibition efficiency (> 90%), with the ability to maintain inhibition capacity over time.
- (3) Good dispersibility, enhanced mechanical properties of the organic coating, and suitability for application in the fabrication of corrosion-protective coatings based on epoxy.

## **3. Thesis research content**

- (1) Study the influence of pH, stirring rate, and hydrothermal temperature on the morphology and particle size of LDH, thereby determining the optimal

conditions for synthesizing LDH with uniform morphology and size.

(2) Controlled synthesis of LDH nanosheets: studying the influence of seed separation and dispersion on the crystal growth orientation of the material; controlling the material size and evaluating the long-term stability of the nanosheet systems.

(3) Synthesis and characterization of LDH nanosheet systems carrying the organic corrosion inhibitor BTSA (LDH-BTSA-ns): studying the influence of anion exchange conditions (time of exchange, BTSA:Al<sup>3+</sup> molar ratio) on the structure and corrosion inhibition capacity of LDH nanosheets.

(4) Study the release capability, mechanism, and corrosion inhibition effectiveness of the LDH-BTSA-ns system synthesized via anion exchange method.

(5) Study the application of LDH-BTSA nanosheet structured material in the fabrication of epoxy protective coatings for corrosion protection of steel, and evaluate the protective effectiveness of the coating in a 3% NaCl corrosion environment.

#### **4. New contributions of thesis**

(1) Provide detailed experimental data and a solid scientific basis for successfully synthesizing fully layered 2D LDH nanosheets in aqueous environments using nuclei separation and dispersion methods; establish suitable hydrothermal parameters for fabricating LDH nanosheets with uniform distribution.

(2) For the first time, LDH nanocontainers in the form of nanosheets carrying the organic corrosion inhibitor BTSA were synthesized using the anion exchange method. Based on the BTSA : Al<sup>3+</sup> molar ratio and synthesis conditions, various LDH-BTSA-ns products with different inhibition levels and configurations were carefully designed, ensuring uniform morphology and size.

## CHAPTER 1. OVERVIEW

### 1.1. LDH nanosheet material

#### 1.1.1. Structure of LDH

The structure of LDH materials is specifically described in Figure 1.1, which includes hydroxide layers and interlayer regions. The hydroxide layers form based on  $M^{II}$  and  $M^{III}$  metal hydroxides arranged in octahedral  $M(OH)_6$  layers, where some  $M^{II}$  metals are partially substituted by  $M^{III}$  metals, creating positively charged hydroxide layers similar to the nature of brucite-like structure. The octahedral of hydroxide units are sharing the edges and forming bilayered structures with  $M^{II}/M^{III}$  cations at the center, while hydroxyl groups are distributed over the edges of the octahedral units with hydrogen atoms pointing towards the interlayer region between two brucite-like sheets, where they are interspersed with anions and water molecules. The main characteristic of these materials is the anion exchange ability of the interlayer anions. Depending on the nature of the cations and anions, the density and size of these interlayer structures vary, giving the material its unique properties.

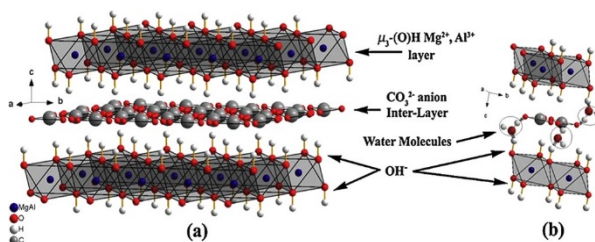


Figure 1.1. Structure of layered double hydroxides

Although LDH has been extensively researched in various fields, its application scope and overall performance are often affected by the stacking of hydroxide layers or even the formation of agglomerates. Exfoliation LDH into individual sheets optimizes the utility of each sheet. In this state, LDH nanosheets exhibit high anisotropy, imparting unique physical and chemical effects that enhance or reveal properties that bulk LDH structures lack or obscure. These nanosheets can serve as basic units for fabricating various functional materials, suitable for both fundamental research and practical applications. The basic structure of LDH

nanosheets is similar to bulk LDH but with a thickness limited to approximately 0.5 – 3 nm, corresponding to crystallite faces with low dimensions (< 6 layers).

### **1.1.2. Size-controlled synthesis method of LDH materials**

Common methods of synthesis LDH include coprecipitation, hydrothermal synthesis, urea hydrolysis, and calcination-reconstruction. Among these, coprecipitation combined with hydrothermal treatment is widely used due to its ability to produce layered double hydroxide (LDH) crystals with several advantages: (i) high uniformity of LDH crystals formation, (ii) stable structure of the LDH product, and (iii) ensuring product purity. Additionally, this method can yield LDH with small particle sizes, offering application benefits. To control the particle size of LDH, several approaches include:

(a) *Controlling crystallization conditions*: some factors influencing the material crystallization process include temperature, hydrothermal time to regulate the particle size of the resulting material.

(b) *Controlling the crystallization environment*: Separating LDH nuclei from the initial reaction environment helps prevent the formation of secondary nuclei during aging, which can affect the distribution of the resulting product.

(c) *Controlling nucleation conditions*: adjusting factors such as stirring speed, contact time, and reaction temperature to form uniform-sized nuclei crystals before proceeding to the aging phase.

### **1.1.3. Synthesis method of LDH nanosheet**

Usually, LDH nanosheets are synthesized using two methods: exfoliation (top-down) and direct synthesis (bottom-up). The exfoliation process is based on the principle of reducing electrostatic bonding forces between the hydroxide layers by gradually increasing the interlayer spacing through the modification of interlayer compositions. Once the interlayer bonding forces of the hydroxide layers are completely disrupted, natural exfoliation occurs or is assisted mechanically. On the other hand, the top-down approach typically involves controlling the nucleation and crystallization process of the material.

(a) *Exfoliation method*: In solvent-based delamination, the process typically involves several stages: (i) initial synthesis of homogeneous LDH using large or weakly polar molecular anions intercalated within the layered structure; (ii) promoting delamination under mechanical agitation such as stirring or ultrasonication in solvents like butanol or formamide.

(b) *Direct synthesis*: Based on the principle of controlling the nucleation and crystal growth process of LDH nanosheets, this method is considered straightforward because it does not require prior synthesis of bulk LDH materials. Compared to the exfoliation method, the direct synthesis method offers several advantages, including the ability to control size and the potential to maintain the nanosheet structure when redispersed in solvent or water. Therefore, this method is more suitable for scaling up production to meet practical applications.

## **1.2. Overview about LDH loaded organic inhibitor system**

### **1.2.1. Anti-corrosion protection mechanism**

LDH demonstrates its protective role for metals based on the physical barrier and exchange anions property, which also supports self-healing properties. When LDH is present in paint or coating layers, it acts as a protective barrier that prevents the permeation of moisture and oxygen, or releases corrosion inhibiting agents in a controlled manner. Dispersed LDH in paint enhances the barrier properties of the organic coating by increasing the diffusion path length of water and corrosive ions to the metal surface. When functionalized with corrosion inhibiting anions, LDH not only physically shields the metal but also enhances its protection efficiency through anion exchange effects.

### **1.2.2. Research status on application of LDH nanosheet in anti-corrosion protective coating**

In the past 5 years, there have been only a few studies applying LDH nanosheets in the fabrication of organic protective coatings against corrosion. Research results show that LDH nanosheets exhibit better dispersion compared to conventional LDH, leading to their high directional alignment within polymer

matrices and forming a high-density barrier layer that effectively prevents the penetration of corrosion agents such as  $\text{Cl}^-$ ,  $\text{O}_2$  or  $\text{H}_2\text{O}$ .

## **CHAPTER 2. EXPERIMENT**

### **2.1. Chemicals**

$\text{MgCl}_2 \cdot 6\text{H}_2\text{O}$  98%,  $\text{AlCl}_3 \cdot 6\text{H}_2\text{O}$  99%, NaOH 98% was purchased from Alfa Aesar.  $\text{NaC}_3\text{H}_5\text{O}_3$  60%,  $\text{Na}_2\text{CO}_3$  99,8%,  $\text{C}_2\text{H}_5\text{OH}$  99,9 % và NaCl 99,5% was supplied from Scharlau. The organic inhibitor BTSA 98,5% was distributed by Zhengzhou HQ Material, and  $\text{N}_2$  99,999% air was purchased from SunAir. Epoxy D.E.R 671-X75 (450 – 500 g/eq), Polyamine XUS 19036.00 (34 g/eq) from Dow Chemical.

### **2.2. Size-controlled synthesis of LDH**

The LDH material is synthesized using a coprecipitation method combined with hydrothermal treatment and stirring. The particle size of LDH is controlled by regulating the hydrothermal temperature under fixed synthesis conditions at pH 10 and 24 hours of hydrothermal treatment.

### **2.3. Preparation of LDH nanosheet**

LDH nanosheets are synthesized using an approach involving seed separation and dispersion. After coprecipitation, the seed crystals are separated from the initial reaction environment and redispersed using high-speed homogenization equipment. The seed crystals undergo restructuring and development in a hydrothermal environment. To control the size of the nanosheets, the hydrothermal temperature is adjusted typically within the range of 80 to 125°C.

### **2.4. Synthesis of LDH loaded organic inhibitor (BTSA)**

LDH nanosheets loading organic corrosion inhibitors like BTSA (LDH-BTSA-ns) are synthesized using the anion exchange method.

### **2.5. Preparation of epoxy coating on carbon steel S45C**

- The steel sample is cleaned thoroughly before applying the epoxy coating.
- LDH-BTSA composite is mechanically blended into the epoxy matrix.

-The steel panel is immersed in the epoxy/LDH-BTSA mixture and left to dry for 14 days to achieve the desired epoxy coating thickness of  $25 \pm 2 \mu\text{m}$ .

## **2.6. Evaluation the inhibitor release and corrosion protection**

The corrosion inhibitor release capacity is determined using UV-Vis spectroscopy. The sample is dispersed in NaCl solution, filtered through a  $0.45 \mu\text{m}$  PTFE membrane, and then standardized with ethanol. The BTSA content in the sample is determined based on a calibration curve.

The corrosion inhibition efficiency of LDH is determined using Tafel polarization curves and electrochemical impedance spectroscopy (EIS) on a VSP Biologic instrument (France). A three-electrode system is used, consisting of: (1) an Ag/AgCl reference electrode (3 M KCl); (2) a platinum mesh as the counter electrode; and (3) a steel working electrode immersed in 0.1 M NaCl solution.

## **2.8. The analysis of epoxy coating**

Mechanical properties of the coating: The thickness, contact angle, adhesion, and degree of peeling of the coating are determined using the MINITest 600, OCA15EC, PosiTect AT-A, and CC2000 devices from TQC Sheen according to ISO 2409-2013. Accelerated corrosion testing is conducted on the CCX3000 salt spray chamber from ATLAS (USA) according to ASTM B117. The impedance spectra of the coated steel samples are measured using the Biologic VSP electrochemical device.

# **CHAPTER 3. RESULTS AND DISCUSSION**

## **3.1. Size-controlled of LDH**

### **3.1.1. The influence of pH on morphology and particle size of LDH**

The co-precipitation process in the pH range of 8-12 does not significantly affect the crystal structure of the material (Figure 3.1a). The LDH samples clearly exhibit the typical vibrations of layered double hydroxide materials, demonstrating the stability of the synthesis method even when performed at

different pH values (Figure 3.1b). The synthesized samples display characteristic diffraction peaks corresponding to the (012), (018), and (110) planes of LDH.

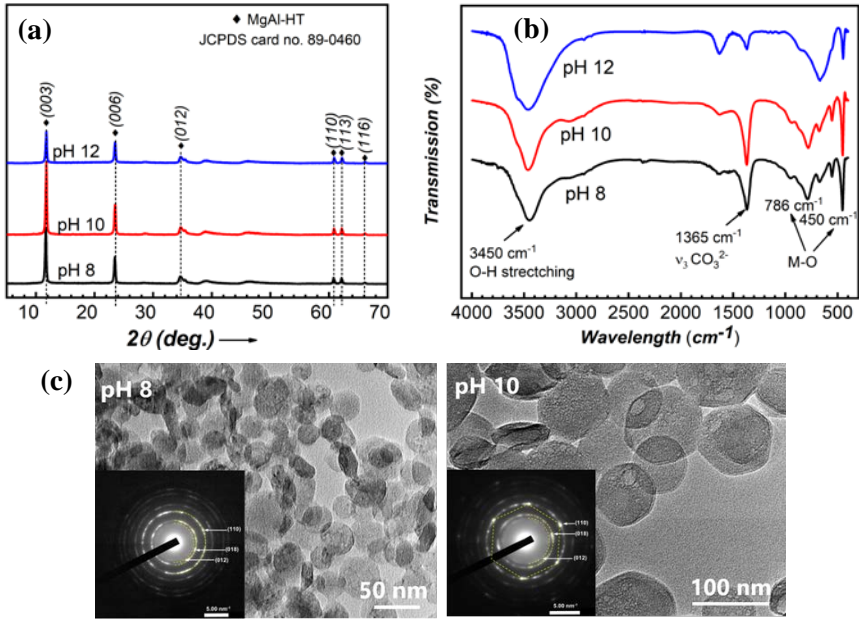


Figure 3.1. XRD (a) and FTIR (b) results of LDH samples synthesized at various pH, (c) TEM & SEAD mode of LDH synthesized at pH 8, 10.

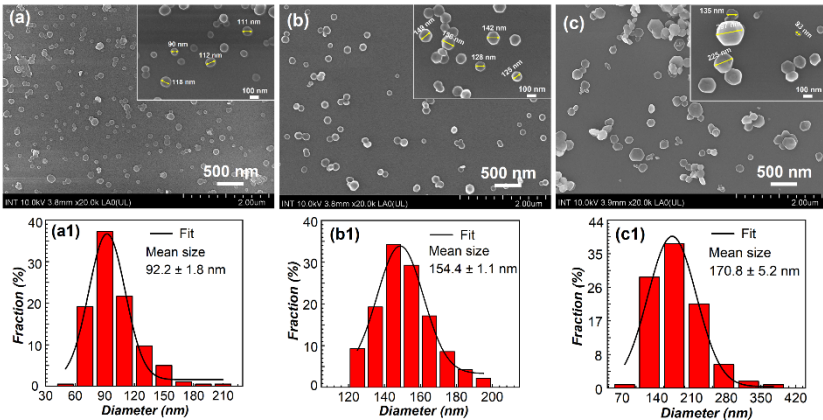


Figure 3.2. FE-SEM images and distribution graph of LDH synthesized at pH 8 (a,a1), 10 (b,b1) & 12 (c,c1)

Maintaining the pH and stirring conditions during the hydrothermal treatment is essential for controlling the size and uniform shape of the nanoparticles. At low pH, LDH exhibits flat particles with rounded, thin edges, with an average particle diameter ( $D_{TB}$ ) of approximately  $92.2 \pm 1.8$  nm (Figure 3.2-a,a1). As the pH increases to 10, the nanoparticles grow larger and tend to develop a more defined hexagonal morphology, with a  $D_{TB}$  of about  $152.4 \pm 1.1$  nm. At pH 12, the formed nanoparticles exhibit irregular shapes and sizes with an average  $D_{TB}$  of around 170.8 nm, accompanied by a large error margin of  $\sim 5.2$  nm (Figure 3.2-c,c1).

### 3.1.2. Influence of the hydrothermal agitation on morphology of LDH

In the case where diffusion occurs slowly (without stirring), LDH growth is disoriented and uneven. With the support of stirring, cation diffusion becomes more uniform during the restructuring and crystal growth stages, leading to the formation of LDH particles with uniform size (Figure 3.3).

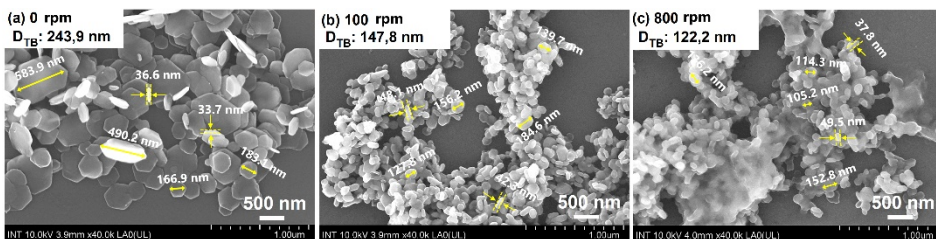


Figure 3.3. SEM image of LDH hydrothermally at various stirring speed

### 3.1.3. The influence of hydrothermal temperature on particle size of LDH

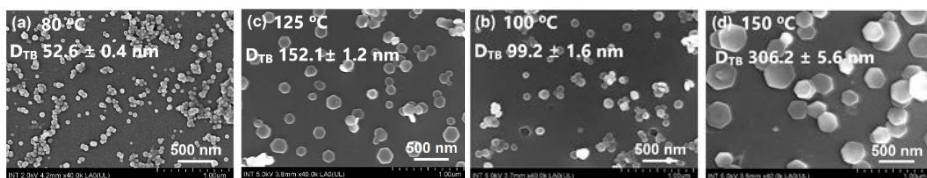


Figure 3.4. SEM images of LDH hydrothermally at various temperature

When the hydrothermal temperature is increased from 80 to 150 °C, the average particle diameter ( $D_{TB}$ ) of the material increases from  $\sim 50$  to 300 nm. The shape and size of LDH are significantly influenced by stirring and temperature factors (Figure 3.4). When only aging is performed (80 °C), the particles formed are

spherical with a small size of about 50 nm. The hydrothermal process ( $\geq 100\text{ }^{\circ}\text{C}$ ) facilitates the formation of nanoparticles with a hexagonal shape.

### 3.2. Synthesis of LDH nanosheets using the separation and division approaches

#### 3.2.1. Morphology of the LDH nanosheet

The LDH nanosheets exhibit a round morphology with very faint contrast in TEM images (Figure 3.5a). The LDH-nanos colloidal system clearly displays the Tyndall effect when a laser beam is directed from the side (Figure 3.5b) and demonstrates thixotropic behavior when left undisturbed in a static state for 24 hours (Figure 3.5c). The LDH nanosheets are dispersed discretely, with a minimum thickness reaching as low as 1.42 nm (Figure 3.5d, e, f).

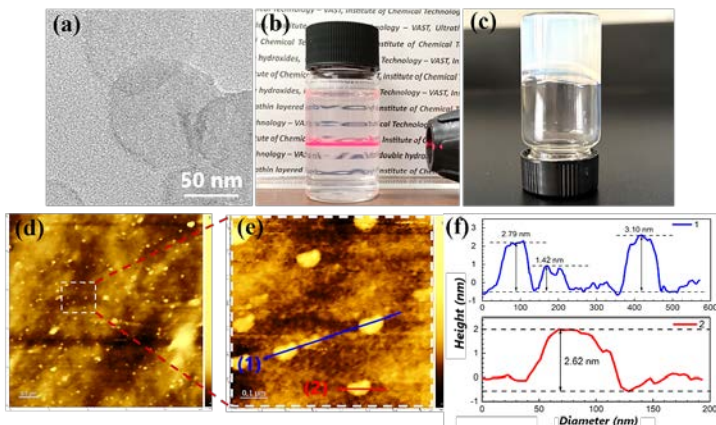


Figure 3.5. TEM (a), visual images (b,c) and AFM results of synthesized by separation and division approaches

#### 3.2.2. The composition and structure of LDH nanosheet

EDS results indicate that the basic components of LDH nanosheets include C, O, Mg, Al, and Cl with respective molar percentages of 8.25%, 60.89%, 16.40%, 8.24%, and 6.21%. The Mg/Al molar ratio is 1.99, similar to the theoretical molar ratio used in synthesis. LDH-nanos exhibits characteristic vibrations of -OH, COO-groups in the layered structure, and M-O in the brucite layer (Figure 3.6a). The interlayer spacing of the LDH nanosheet is 0.784 nm (Figure 3.6b). The structure of the LDH nanosheet can be described as shown in Figure 3.7c.

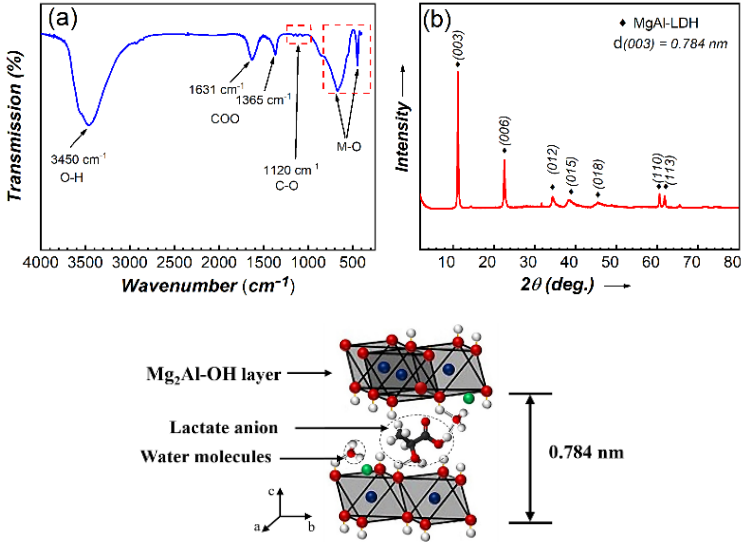


Figure 3.6. (a) FTIR and (b) XRD results (c) simulated structure of LDH-ns

### 3.2.3. The influence of SAD approach on the formation of LDH nanosheet

To clarify the mechanism and impact of seed dispersion, both treated (LDH-CI-H) and untreated homogenized samples were prepared simultaneously for comparison. The seed/hydroxide aggregates in the LDH-CI-F sample were effectively dispersed under hydraulic shear forces, resulting in evenly dispersed seed/hydroxide clusters on the silicon wafer substrate (Figure 3.7-a,b). The LDH-CI-F suspension exhibited a high polydispersity index (PI: 0.638), with an average hydrodynamic size of around 1819.8 nm. In contrast, LDH-CI-H showed a more uniform particle size distribution, with a lower PI (0.349) and an average hydrodynamic size of 363.8 nm (Figure 3.7e).

Table 3.1. Morphology, average size, zeta potential and aspect ratio of synthesized LDH nanosheet

Temperature	$D_{TB}$ (nm)	PI	Zeta potential (mV)	AR
80 °C	77.4	0.171	+61,7	54.5
100 °C	115.4	0.195	+72,1	81.3
125 °C	168.4	0.180	+73,9	118.6
150 °C	212.5	0.131	+75,6	149.6

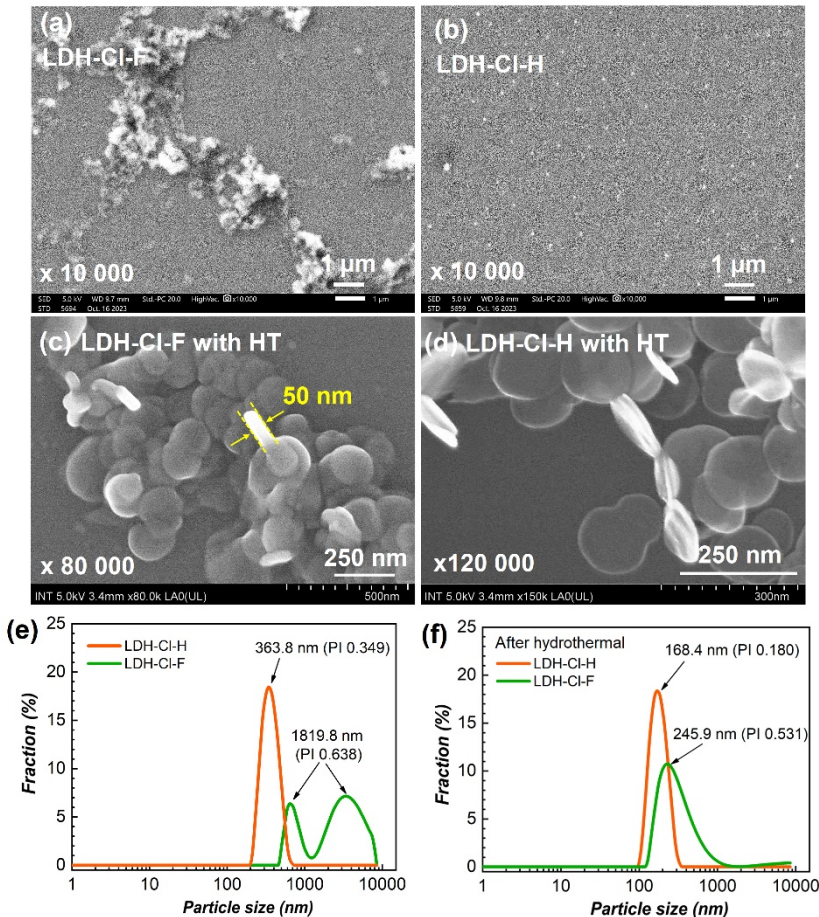


Figure 3.7. SEM image of LDH-CI-F (a), LDH-CI-H (b) precursors and LDH-CI-F (c), LDH-CI-H (d) after hydrothermal at 125°C and DLS size distribution of precursors and LDH systems after hydrothermal.

After thermal treatment, the DLS particle size of LDH-CI-F decreases due to dissolution of hydroxide components and transformation into crystalline LDH structure through diffusion and crystallization processes. There is aggregation of LDH nano particles observed in the LDH-CI-F system post-thermal treatment, with particle thickness measured around 50 nm (Figure 3.8a). In contrast, LDH-CI-H shows a thin, sheet-like morphology on the silicon wafer (Figure 3.8b). LDH-CI-H exhibits narrow size distribution, averaging approximately 168.4 nm (Figure 3.8c), with a low polydispersity index (PI) of 0.180. LDH-CI-F after

thermal treatment shows broader size distribution (PI  $\sim 0.531$ ) and larger size ( $\sim 245.9$  nm), indicating the aggregation during the formation and growth of particle. LDH crystals preferentially develop along the horizontal planes ( $a$ ,  $b$  axes) compared to the  $c$ -axis. The LDH nanosheet colloidal system exhibits a zeta potential value of  $+73.9$  mV, significantly higher than the non-homogeneous LDH system ( $+35.2$  mV), highlighting the stability of the resulting LDH nanosheet (Table 3.1).

### 3.3. Synthesis of LDH nanosheet loaded organic inhibitor

After the ion exchange with the corrosion-inhibiting anion BTSA<sup>2-</sup>, the diffraction angle of the (003) plane of the nanosheet material shifted from  $2\theta = 11.28^\circ$  to  $5.38^\circ$  (Figure 3.8a), indicating an expansion of the interlayer distance in the LDH-BTSA-ns system from 0.784 nm to 1.644 nm. The presence of the conjugated C–H group in the aromatic ring (at a wavenumber of  $758\text{ cm}^{-1}$ ) and the shift of the COO<sup>-</sup> functional group's wavenumber to a lower position compared to the original BTSA (wavenumbers  $1574$  and  $1402\text{ cm}^{-1}$ ) confirms the incorporation of BTSA into the LDH interlayer (Figure 3.8b).

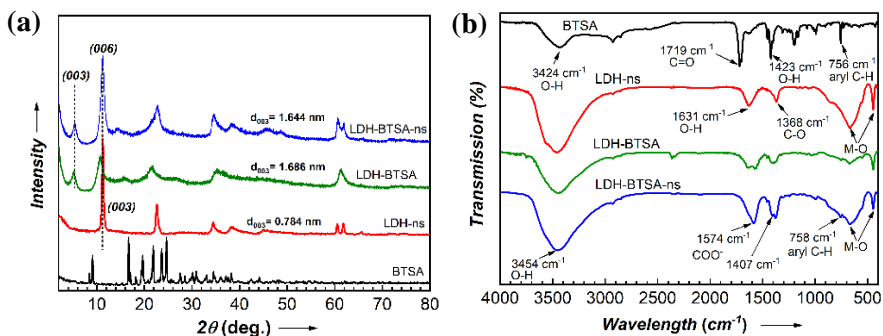


Figure 3.8. XRD pattern (a), FTIR spectra (b) of BTSA, LDH-ns, LDH-BTSA-ns, LDH-BTSA-c

The BTSA content in the structure, determined via TGA and UV-Vis, was approximately 38 wt% after 24 hours of ion exchange (Figure 3.9-a,b). XRD analysis revealed that the BTSA content could influence the crystal structure of the formed LDH-BTSA-ns. More than one crystal phase was formed at an

Al:BTSA molar ratio of 1:3. The diffraction signal of the (003) plane of phase #2 (at  $2\theta = 10.6^\circ$ ) overlapped with the diffraction region of the (006) plane of phase #1 at  $2\theta = 11.2^\circ$  (Figure 3.10-a,b). The two-phase structure of LDH-BTSA-ns is illustrated in Figure 3.10c.

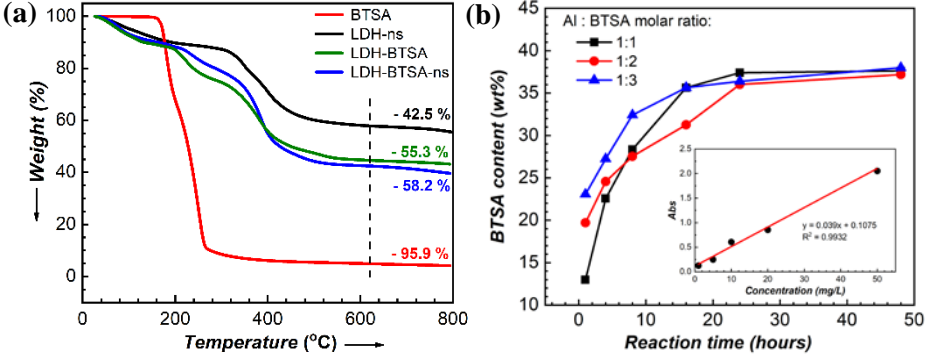


Figure 3.9. (a) TGA pattern and (b) amount of BTSA intercalated by time

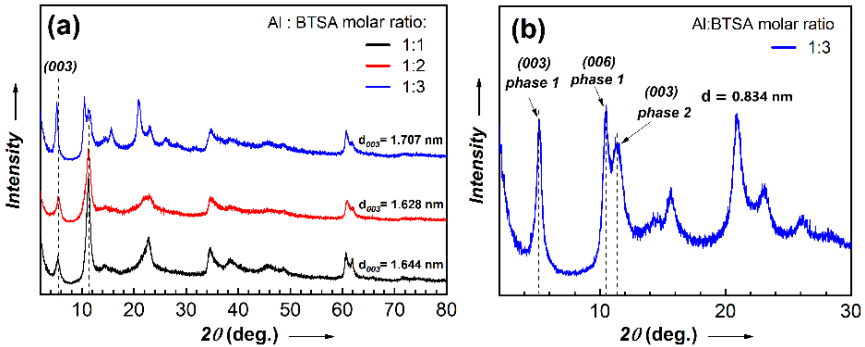


Figure 3.10. XRD patterns of LDH-BTSA-ns preparation at various Al:BTSA ratio and signal at (00l) planes of sample synthesis at molar ratio of 1:3

### 3.4. Study of the corrosion inhibition mechanism of LDH-BTSA-ns

#### 3.4.1. Corrosion inhibition release efficiency

The intercalation and deintercalation processes within the LDH structure do not affect the properties of the BTSA inhibitor (Figure 3.11a). The release capability of the corrosion inhibitor is influenced by the NaCl concentration. After 24 hours of exchange, the release percentages of the organic compound were 21.96%, 41.77%, and 57.63% corresponding to increasing NaCl concentrations (Figure

3.1b). After the equilibrium of the exchange reaction, BTSA remains stored within the nano reservoirs, as evidenced by XRD and FTIR spectra (Figure 3.12).

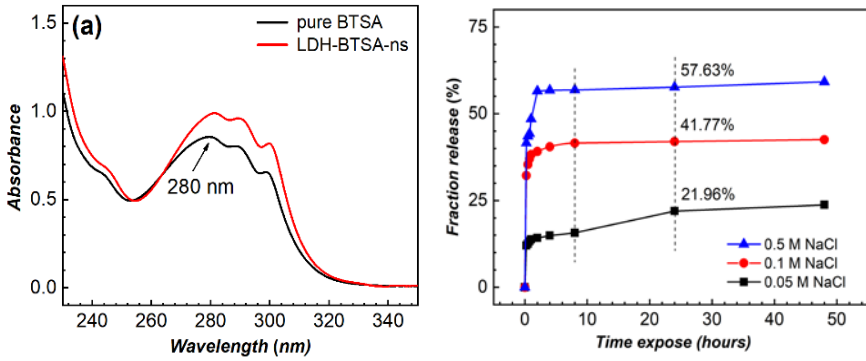


Figure 3.11. (a) UV-vis spectrum of BTSA free and BTSA release from LDH-BTSA-ns; (b) % BTSA release in NaCl solution

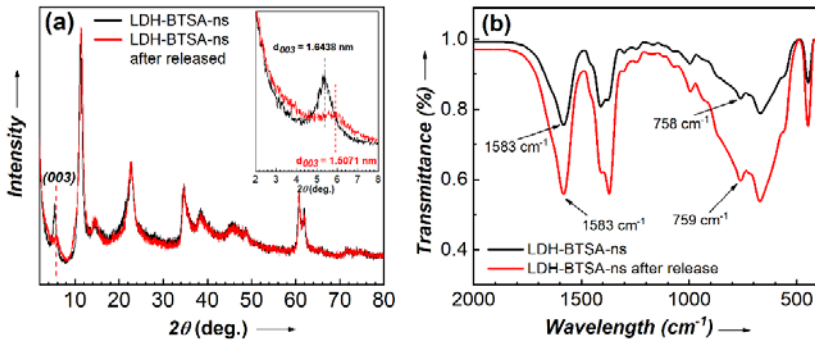


Figure 3.12. XRD patterns (a) and FTIR spectrums (b) of LDH-BTSA-ns before and after immersed in NaCl 0,1 M solution

### 3.4.2. Corrosion inhibition release efficiency

The corrosion potential ( $E_{\text{corr}}$ ) values of steel electrodes immersed in NaCl solutions without inhibitors and with LDH-ns, LDH-BTSA, LDH-BTSA-ns at 3 g/L, and BTSA at 0.005M were -613.589, -555.169, -489.794, -439.462, and -335.079 mV, respectively (Figure 3.13). The corrosion current density ( $i_{\text{corr}}$ ) in the solution containing LDH-BTSA-ns ( $1.866 \mu\text{A}\cdot\text{cm}^{-2}$ ) was significantly lower compared to the solution with LDH-ns ( $12.987 \mu\text{A}\cdot\text{cm}^{-2}$ ) and the blank sample ( $19.202 \mu\text{A}\cdot\text{cm}^{-2}$ ). The inhibition efficiency of LDH-BTSA-ns reached 90.3% after 2 hours of immersion.

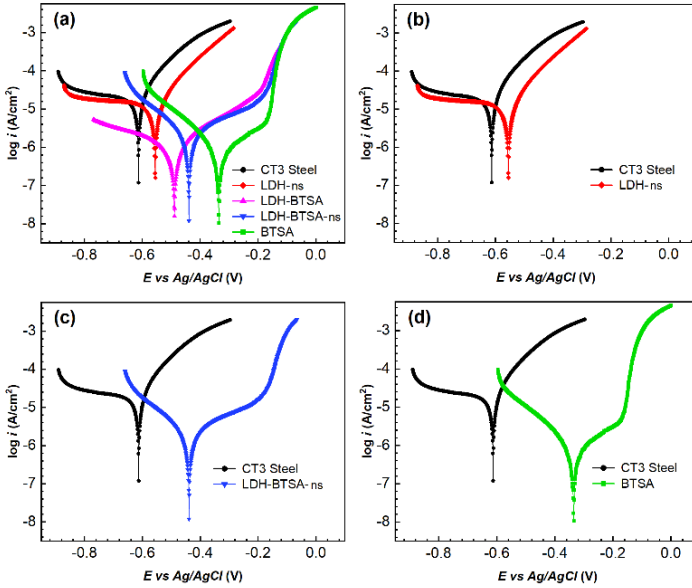


Figure 3.13. Tafel curves SC45 electrode after 2 hours of immersion in NaCl 0.1M blank solution and consist of LDH-ns, LDH-BTSA-ns 3 g/L and  $\text{Na}_2\text{BTSA}$  0,005M

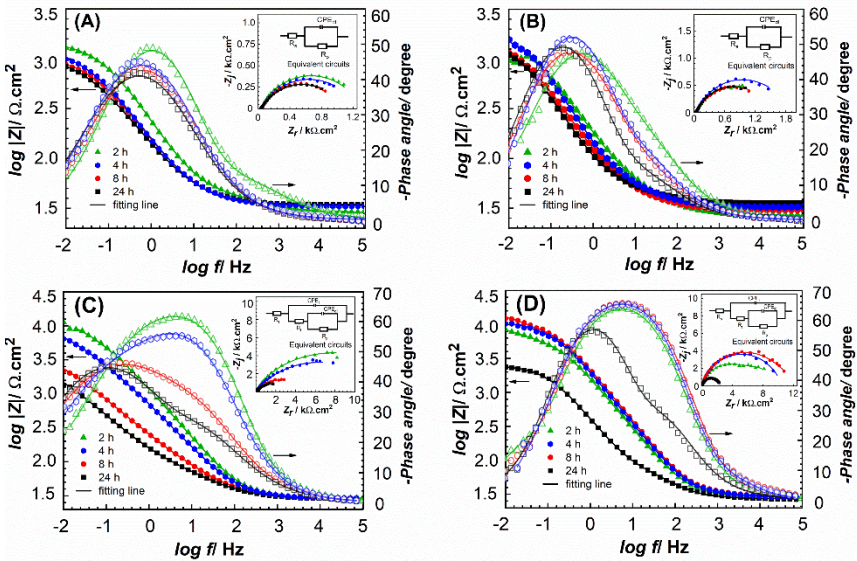
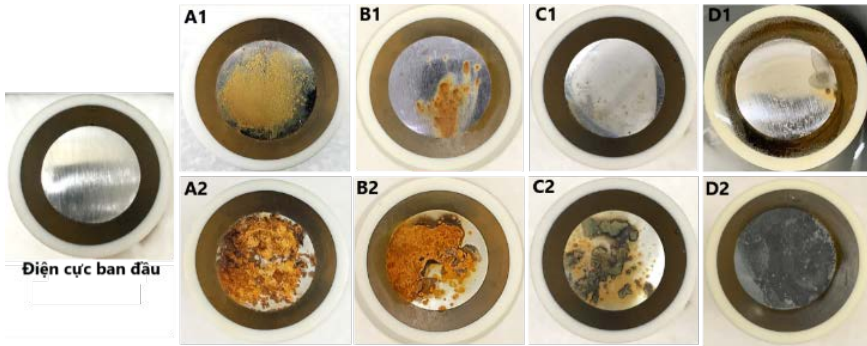


Figure 3.14. Bode plots và Nyquist plots (inset images) of S45C electrode after immersion in NaCl 0.1 M blank (A) and consist of LDH-ns (B),  $\text{Na}_2\text{BTSA}$  0,005 M (C) và LDH-BTSA-ns 3 g/L (D) by time.

After 2 hours of immersion in blank NaCl solution and solutions containing LDH-nz and LDH-BTSA-nz at 3 g/L, the  $R_p$  values were 1300, 1571, and 6905  $\Omega \cdot \text{cm}^2$ , respectively (Figure 3.14). The  $R_p$  value of the electrode immersed in the 0.005M BTSA solution was very high, reaching 14190  $\Omega \cdot \text{cm}^2$ . However, this value significantly decreased with increasing immersion time, dropping to 9979, 4935, and 2409  $\Omega \cdot \text{cm}^2$  after 4, 8, and 24 hours, respectively, indicating the rapid consumption of BTSA on the electrode surface. In contrast, the  $R_p$  value of the solution containing LDH-BTSA-nz increased to 9703 and 11271  $\Omega \cdot \text{cm}^2$  after 4 and 8 hours of immersion. After 24 hours of immersion, the  $R_p$  value decreased due to the consumption of the inhibitor molecules on the metal surface but still maintained a high value of 3270  $\Omega \cdot \text{cm}^2$ .



*Figure 3.15. The optical images of S45C electrode after 2 and 24 hours immersion in NaCl 0,1 M blank solution (A1,A2) and consist of LDH-nz 3 g/L (B1,B2), Na<sub>2</sub>BTSA 0,005 M (C1,C2) và LDH-BTSA-nz 3 g/L (D1,D2)*

After 24 hours of immersion, electrodes immersed in the blank solution and the LDH-nz solution exhibited clear and uniform rust spots. The sample immersed in BTSA showed rust layers and widely spread gray-green regions on the surface. In contrast, no rust spots were observed on the sample in LDH-BTSA-nz (Figure 3.15). In the absence of inhibitors, corrosion product crystals were clearly observed, covering the electrode surface (Figure 3.16-A, B). The elemental composition was predominantly iron and oxygen, with contents of 69.3% and 28.5%, respectively, confirming the formation of iron oxide on the steel electrode surfaces. In the presence of LDH-BTSA-nz, plate-like particles similar to

nanosheets were easily observed covering the electrode surface (Figure 3.16-C, D). SEM and EDS analysis results indicated the formation of a protective barrier layer on the electrode surface. The protection mechanism of LDH-BTSA-ns is illustrated in Figure 3.17.

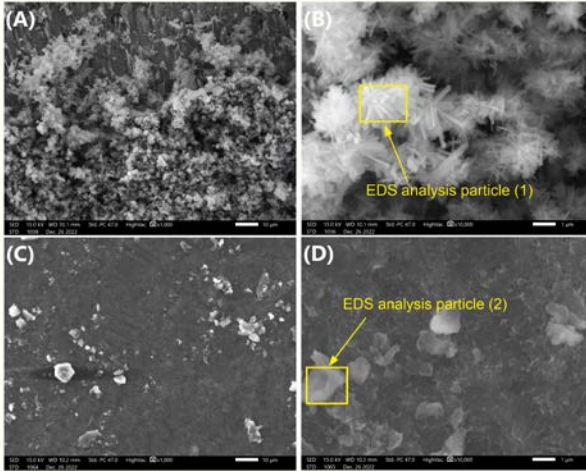


Figure 3.16. SEM image of surface electrodes after 24 hours immersion in NaCl 0,1 M blank solution (A,B) và consist of 3 g/L LDH-BTSA-ns (C,D)

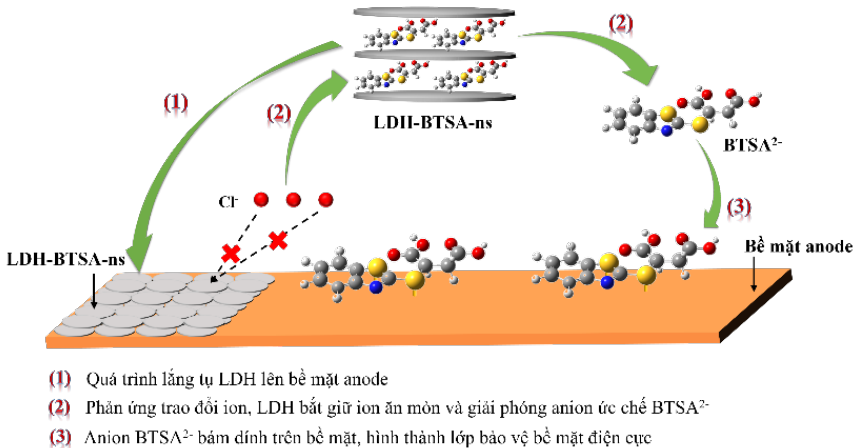


Figure 3.17. The mechanism corrosion protection of LDH-BTSA-ns

### 3.5. Fabrication of epoxy based anti-corrosion coating

#### 3.5.1. Fabrication and physical properties coating films

The paint coatings were applied by immersion onto carbon steel panels measuring 150 x 100 x 200 mm, with a film thickness after 14 days of curing of

$25 \pm 2 \mu\text{m}$ . All films exhibited similar appearances (Figure 3.18), adhered well without signs of detachment during the cross-cut and classification test, achieving group 0 (the highest rating) according to TCVN 2097:2015. The contact angles of the Ep-0, Ep/LDH-ns, Ep/LDH-BTSA, and LDH-BTSA-ns films were  $45.7^\circ$ ,  $80.2^\circ$ ,  $71.9^\circ$ , and  $78.2^\circ$  respectively.

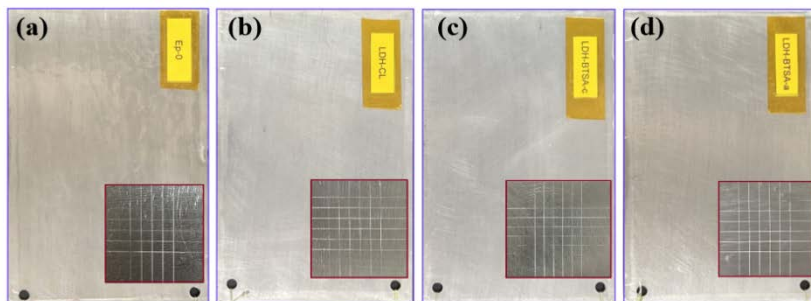


*Figure 3.18. Visual appearance of the fabricated paint films (a) Ep-0, (b) Ep/LDH-ns, (c) Ep/LDH-BTSA, and (d) EP/LDH-BTSA-ns, and attached images of the cross-cut test conducted according to the square grid method*

### 3.5.2. The film's protective efficiency by EIS

After 3 days of immersion, the Nyquist curve of the epoxy coatings consistently show one main semicircle at high frequencies, characteristic of the film properties (Figure 3.19a-d). This indicates diffusion of the electrolyte solution into the epoxy film structure through defects or voids formed during fabrication, but no surface corrosion has occurred yet. After 21 days of immersion, the Nyquist total resistance spectra of the Ep-0, Ep/LDH-ns and Ep/LDH-BTSA-c samples reveal a second semicircle at low frequencies (Figure 3.19a-c), indicating corrosion processes at the metal surface. The Ep/LDH-BTSA-ns sample still exhibits only one defined semicircle (Figure 3.19-c1), demonstrating the effective barrier capability of the nanosheet structure within the paint films.

After 3 and 7 days, the  $Z_{100\text{mHz}}$  values of the Ep-0 sample were  $6.2$  and  $5.8 \times 10^8 \Omega \cdot \text{cm}^2$ , respectively. These values then rapidly decreased to  $5.2 \times 10^7 \Omega \cdot \text{cm}^2$  and  $3.7 \times 10^6 \Omega \cdot \text{cm}^2$  after 21 and 42 days of immersion. Additionally, the Bode plot exhibits a pronounced curve in the low-frequency region, indicating significant

deterioration of the film over the immersion period (Figure 3.20). The Ep/LDH-ns coating, after 7 days of immersion, exhibited a significant drop in  $Z_{100\text{mHz}}$  value compared to the initial immersion time, decreasing to approximately  $3.7 \times 10^8 \Omega \cdot \text{cm}^2$ . This value further reduced to  $2.5 \times 10^6 \Omega \cdot \text{cm}^2$  after 42 days of immersion.

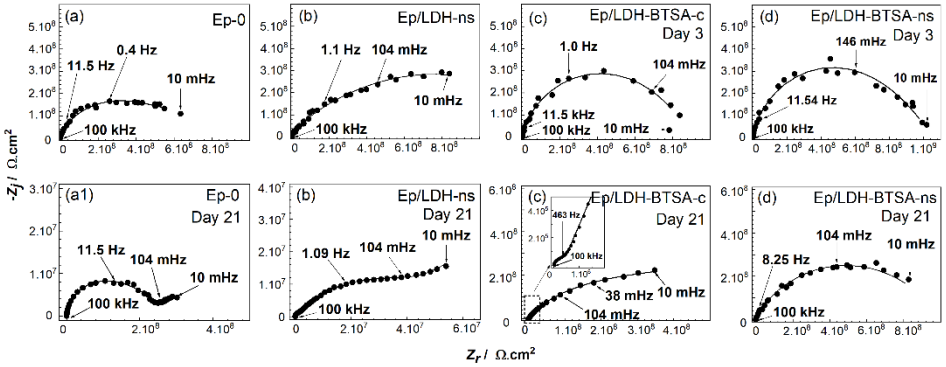


Figure 3.19. Nyquist plot of Ep-0, Ep/LDH-BTSA, Ep-LDH-BTSA-ns after 1 (a, b, c) and 21 days (a1, b1, c1) immersion

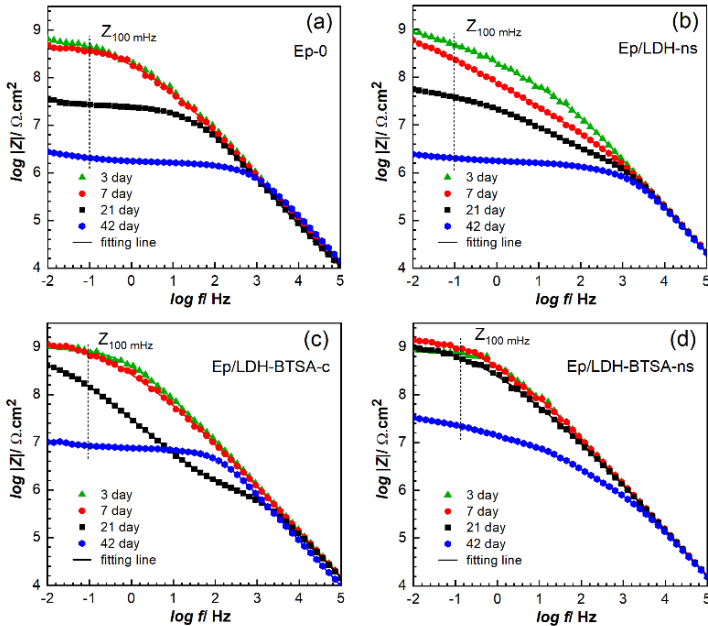


Figure 3.20. Bode plot of Ep-0, Ep/LDH-BTSA, Ep-LDH-BTSA-ns after 3, 7, 21 and 42 days immersion in NaCl 3% solution

The Ep/LDH-BTSA-c and Ep/LDH-BTSA-ns coatings both initially exhibited high  $Z_{100\text{mHz}}$  values, at  $8.8 \times 10^8$  and  $9.5 \times 10^8 \Omega \cdot \text{cm}^2$ , respectively. After 7 days of immersion, the  $Z_{100\text{mHz}}$  value of the Ep/LDH-BTSA-c coating slightly decreased to  $8.1 \times 10^8 \Omega \cdot \text{cm}^2$ , and subsequently reduced to  $2.1 \times 10^8 \Omega \cdot \text{cm}^2$  and  $9.1 \times 10^6 \Omega \cdot \text{cm}^2$  after 21 and 42 days of immersion. The reduction in impedance for the Ep/LDH-BTSA-c coating was less than that of the Ep-0 coating, demonstrating the effectiveness of the nanosheet structure.

In contrast, the Ep/LDH-BTSA-ns coating showed no significant decrease in  $Z_{100\text{mHz}}$  value over the 21 days immersion period. Furthermore, after 7 days, the  $Z_{100\text{mHz}}$  value increased to  $1.6 \times 10^9 \Omega \cdot \text{cm}^2$ . This indicates the superior corrosion inhibition of the nanosheet material compared to the bulk material when dispersed in the polymer matrix. After 42 days of immersion, the  $Z_{100\text{mHz}}$  value of Ep/LDH-BTSA-ns remained at  $3.3 \times 10^7 \Omega \cdot \text{cm}^2$ , which is approximately 4 times higher than that of Ep/LDH-BTSA-c, 9 times higher than Ep-0, and 13 times higher than Ep/LDH-ns.

### **3.5.3. Accelerated corrosion testing results**

The results of the salt spray test demonstrate that the epoxy paint film containing corrosion-inhibiting nanosheet structures provides superior corrosion protection effectiveness compared to the paint using bulk materials. The corrosion intensity with the Ep/LDH-BTSA-ns sample is significantly lower, and the film remains intact without any signs of blistering. After 360 hours of testing, the rust width measurements for samples Ep-0, Ep/LDH-ns, Ep/LDH-BTSA, and Ep/LDH-BTSA-ns are  $902.6 \pm 8.7$ ;  $1006.4 \pm 9.2$ ,  $586.3 \pm 6.9$ ; and  $262.7 \pm 4.2 \mu\text{m}$ , respectively. The Ep/LDH-BTSA-ns sample showed the best metal corrosion protection capability according to ASTM D1654-08 standard (level 9).

## **CHAPTER 4. CONCLUSION**

This thesis has achieved its research objectives with the following key results:

(1) The thesis successfully developed a synthesis process with controlled morphology and size of LDH-CO<sub>3</sub> materials using a combined coprecipitation and hydrothermal method with agitation. The study clarified the influence of particle size and distribution on the durability of the nanostructured LDH-CO<sub>3</sub> system, where LDH-CO<sub>3</sub> with an average size of ~150 nm achieved the highest zeta potential, exceeding +70 mV.

(2) Propose an efficient and simple process for synthesizing LDH nanosheets with uniform morphology and low crystallite size (~1.42 nm) equivalent to 2-3 unit cells, low polydispersity index (PI ~ 0.1), high zeta potential (> +60 mV), and high stability (> 90 days). The particle size distribution (PSD) can be controlled within 77.2 – 212.5 nm using hydrothermal treatment with stirring at temperatures ranging from 80 – 150 °C.

(3) Constructed synthesis conditions with controlled corrosion inhibition content in the double-layered structure of LDH using anion exchange methods. Achieved maximum corrosion inhibition content of 37.56%, while ensuring uniformity in morphology and size of the product.

(4) Study the application of LDH-BTSA nanosheets in the fabrication of epoxy coatings for corrosion protection of steel. The presence of LDH-BTSA-ns (at a concentration of 3%) significantly improved the mechanical and physical properties of the epoxy coating: (i) the relative hardness of the coating increased from 0.68 to 0.79; (ii) adhesion strength increased from 1.86 to 2.56 MPa; (iii) the contact angle increased from 45.7° to 78.2°.

(5) The nanosheet material system carrying corrosion inhibitors offers better shielding compared to bulk materials. After 42 days of immersion in 3% NaCl solution, the total impedance modulus  $Z_{100\text{mHz}}$  of the Ep/LDH-BTSA-ns sample remained at  $3.3 \times 10^7 \Omega \cdot \text{cm}^2$ , which is 4 times higher than Ep/LDH-BTSA-c and 9 times higher than Ep-0. The Ep/LDH-BTSA-ns coating demonstrated superior protective performance after 360 hours of salt spray testing.

**LIST OF SCIENTIFIC WORKS RELATED TO THE THESIS THAT  
HAVE BEEN PUBLISHED**

1. **Minh Vuong Phan**, Thi Kim Thoa Tran, Quynh Nhu Pham, Manh Huy Do, Thi Hong No Nguyen, Minh Ty Nguyen, Thanh Thao Phan, Thi Xuan Hang To. *Controllable synthesis of layered double hydroxide nanosheets to build organic inhibitor-loaded nanocontainers for enhanced corrosion protection of carbon steel*. Nanoscale Advances, **2024** 6(2), 606-619. (SCIE, Q1, IF~4.6).
2. **Minh Vuong Phan**, Thi Kim Thoa Tran, Quynh Nhu Pham, Manh Huy Do, Thi Hong No Nguyen, Minh Ty Nguyen, Thanh Thao Phan, Thi Xuan Hang To. *Controllable Synthesis of Hollow Silica Nanoparticles Using Layered Double Hydroxide Templates and Application for Thermal Insulation Coating*. ACS Omega, **2023**, 8(34), 31399-31409. (SCIE, Q1, IF~3.7).
3. **Phan Minh Vuong**, Tran Thi Kim Thoa, Pham Quynh Nhu, Nguyen Thi Hong No, Nguyen Minh Ty, Do Manh Huy, Phan Thanh Thao, To Thi Xuan Hang. *Controllable synthesis of uniform MgAl-hydrotalcite nanoplates and their size-dependent on anti-corrosion properties of carbon steel*. Vietnam Journal of Chemistry, **2022**, 60, 32-40. (Scopus, Q3).